Feasibility of Imaging Pentose Cycle Glucose Metabolism in Gliomas with PET: Studies in Rat Brain Tumor Models

Alexander M. Spence, Michael M. Graham, Mark Muzi, Scott D. Freeman, Jeanne M. Link, John R. Grierson, Finbarr O'Sullivan, Donna Stein, Gregory L. Abbott and Kenneth A. Krohn

Departments of Neurology, Radiology and Statistics, University of Washington School of Medicine, Seattle, Washington

The feasibility of imaging pentose cycle (PC) glucose utilization in human gliomas with PET was explored in two rat glioma models by means of glucose radiolabeled in either the carbon-1 (C-1) or carbon-6 (C-6) position. **Methods:** In vitro, monolayers of T-36B-10 glioma, tissue slices of intracerebral glioma grafts or slices of normal brain were fed [1-^{14}C]glucose or [6-^{14}C]glucose, and the generated [^{14}C]CO_2 was trapped to quantitate the ratio of [^{14}C]CO_2 from ^{14}C-1 versus ^{14}C-6. In vivo, rats bearing grafts of either T-36B-10 or T-C6 rat gliomas at six subcutaneous sites received simultaneous intravenous injections of either [1-^{11}C]glucose and [6-^{14}C]glucose, or [1-^{14}C]glucose and [6-^{11}C]glucose. Tumors were excised between 5 and 55 min postinjection to quantify tracer uptake while arterial plasma was collected to derive time-activity input curves. **Results:** In vitro, the C-1/C-6 ratio for CO_2 production from T-36B-10 monolayers was 8.8 ± 0.4 (s.d.), in glioma slices it was 6.1 ± 2.1 and in normal brain slices it was 1.1 ± 0.7. PC metabolism in T-36B-10 was 1.8% ± 0.5 of total glucose utilization. In vivo, tumor radioactivity levels normalized by plasma isotopic glucose levels showed that retained C-1 relative to C-6 radiolabeled glucose was significantly lower in both gliomas, 4.9% lower in T-36B-10 ($p < 0.01$) and 4.7% lower in T-C6 ($p < 0.01$). In an additional group of rats bearing T-36B-10 gliomas and exposed to 10 Gy of ^{137}Cs irradiation 4 hr before isotope injection, the C-1 level was 5.6% lower than that for C-6 ($p < 0.05$). These results were analyzed with a model of glucose metabolism that simultaneously optimized parameters for C-1 and C-6 glucose kinetics by simulating the C-1 and C-6 tumor time-activity curves. The rate constant for loss of radiolabeled carbon from the tumors, k4, was higher for C-1 than for C-6 in all groups of rats (19% higher for T-36B-10 unirradiated, 32% for T-36B-10 irradiated and 32% for T-C6 unirradiated). **Conclusion:** Mathematical modeling, Monte Carlo simulations and construction of receiver-operator-characteristic curves show that if human gliomas have a similar fractional use of the PC, it should be measurable with PET using sequential studies with [1-^{11}C]glucose and [6-^{11}C]glucose.

Key Words: rat glioma; glucose metabolism; brain neoplasm; pentose cycle; PET

J Nucl Med 1997; 38:617–624

Several laboratories have measured glucose metabolism in human gliomas with [^{18}F]fluorodeoxyglucose (FDG) and PET (*1–5*). These studies aimed to define tumor grade, localize regions of malignant tissue and assess tumor response to therapy. However, because FDG is not significantly metabolized further by hexokinase than by phosphorylation (*6*), it is impossible to examine glucose metabolism beyond this first step with FDG and PET. With [^{11}C]glucose and PET, selective labeling of the carbon atoms at the C-1 or C-6 position could allow measurement of the fraction of total glucose metabolism used to support biosynthesis via the pentose cycle (PC) versus the fraction used for cellular energetics, thereby providing additional insights into tumor grading and therapeutic response.

These concepts stem from Weber (*7,8*), who reviewed tumor enzymology and reported that flux in the PC is increased in neoplasms relative to normal tissues. In normal adult rat brain, it has been estimated that the PC accounts for about 0.5% (*9*), 1.4% (*10*), 1.5% (*11*), 1.4–2.9% (*12*) or 2.3% (*13*) of glucose utilization. Cultures of normal astrocytes show a PC flux of approximately 1% of the total glucose flux (*14*).

Tumors, on the other hand, tend to show greater PC metabolism. Specifically, the PC enzymes, glucose-6-phosphate dehydrogenase and 6-phosphogluconate dehydrogenase increase in activity in brain tumors with increasing malignancy (*15–18*). Coleman and Allen (*19*) studied the activities of PC enzymes in several ethylnitrosourea-induced rat gliomas and found glucose-6-phosphate dehydrogenase and 6-phosphogluconate dehydrogenase elevated in 6 of 10 and 9 of 10 tumors, respectively, relative to normal brain. These authors also reported data from which the PC fraction can be calculated to be 1.9% and 2.2% in malignant gliomas of the rat spinal cord and brain, respectively (*9*). Kingsley-Hickman et al. (*20*) and Ross et al. (*21*) estimated the fraction of PC glucose metabolism in the rat T-9L gliosarcoma and T-C6 glioma in vitro to be 5.1% and 7.5%, respectively. Lastly, Loreck et al. (*14*) have estimated the PC fraction of glucose metabolism in grade IV human astrocytomas to be 4%.

The PC is important in molecular biosynthesis because it reduces two equivalents of NADP+ to NADPH to maintain glutathione (GSH) in the reduced state (*10,22*) and yields ribulose-6-phosphate (Fig. 1). One potential effect of cancer treatments such as radiotherapy and chemotherapy is to lower GSH and thereby induce PC metabolism. Also, resistance of tumors to therapy may in part be dependent on GSH and its production. High levels of GSH reduce the cytotoxicity of photon irradiation, whereas the presence of O_2 increases this cytotoxicity. Therefore, if it were possible to measure the PC in gliomas in vivo as an indicator of NADPH and GSH production, a better understanding of response or resistance to cytotoxic treatments could emerge.

The biochemical rationale of this article is based on the fate of the carbon atoms of glucose through the PC pathway and the Embden-Meyerhof pathway (EMP) (Fig. 1) (*23*). If PC activity is high in gliomas, metabolism of C-1 radiolabeled glucose will liberate radioactive CO_2 earlier and at a higher rate than will metabolism of C-6-radiolabeled glucose. Conversely, gliomas will retain labeled glucose and its metabolites to a greater degree from C-6-labeled glucose than from C-1-labeled glucose. In the PC, the C-1 of glucose is removed by 6-phosphogluconate dehydrogenase to produce CO_2 and ribulose-5-phosphate. Via the EMP, on the other hand, neither this carbon nor

Received Feb. 22, 1996; revision accepted Jul. 8, 1996.

For correspondence or reprints contact: Alexander M. Spence, MD, Neurology, Box 356465, University of Washington, Seattle, WA 98195.

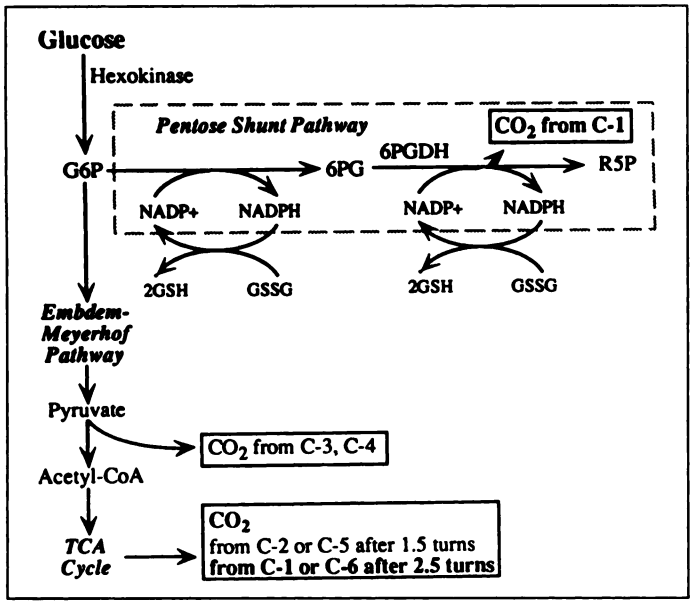

FIGURE 1. Diagram of the chief metabolic pathways of glucose to illustrate where the individual carbon atoms are released as CO_2. G6P = glucose-6-phosphate, 6PG = 6-phosphogluconate, R5P = ribulose-5-phosphate.

any of the other carbons are lost to CO_2 until the three-carbon products of glucose catabolism enter the tricarboxylic acid (TCA) cycle. C-3 and C-4 yield CO_2 when pyruvate is converted to acetyl-CoA; C-2 and C-5 yield CO_2 after 1.5 turns of the TCA cycle; and C-1 and C-6 are liberated as CO_2 only after 2.5 turns of the TCA cycle. In contrast to the PC, once through the EMP and into the TCA cycle, C-1 and C-6 of glucose share essentially the same routes (*23*). Therefore, studies of the fate of C-1- versus C-6-radiolabeled glucose can be used to calculate the relative metabolism of glucose in the PC and the EMP (*24*).

Our experiments in vitro show that there is significantly increased use of the PC in the T-36B-10 rat glioma compared to normal brain. The experiments in vivo with this and the T-C6 rat glioma model (*25*) show that the increase in PC leads to greater loss of C-1 relative to C-6-labeled glucose. With these data plus mathematical modeling, Monte Carlo simulations and construction of receiver-operating-characteristic (ROC) curves, we argue that this level of PC metabolism will be detectable in human gliomas with PET using sequential imaging of C-1 and C-6 [^{11}C]glucose tracers.

MATERIALS AND METHODS

Rat Brain Tumor Model

The origin and maintenance in vitro of the ethylnitrosourea-induced T-36B-10 astrocytic F-344 rat brain tumor model has been reported in detail elsewhere (*26*). T-C6 glioma cells (*25*) were obtained from the American Type Culture Collection (Rockville, MD) and were cultured and maintained in the same manner as the T-36B-10 cultures.

Isotopes, Enzymes and Biochemicals

D-[1-^{14}C]glucose and D-[6-^{14}C]glucose (specific activity, 55 mCi/mmole) were obtained from American Radiolabeled Chemicals (St. Louis, MO). Chemical and radiochemical purity were greater than 99% as analyzed by thin-layer chromatography (*27*), high-performance liquid chromatography (Brownlee Polypore H column eluted with 0.01 *N* H_2SO_4 at 0.3 ml/min) and anion exchange chromatography (*28*). Hexokinase (D-glucose:ATP phosphotransferase, E.C. 2.7.1.1), glucose-6-phosphate dehydrogenase (D-glucose-6-phosphate:NADP+ 1-oxidoreductase, E.C. 1.1.1.49), ATP and NAD+ were purchased from Sigma Chemical Company (St. Louis, MO). Instagel and Soluene-350 (0.5 *N* quaternary ammonium hydroxide in toluene) were acquired from Packard Instrument Company (Downers Grove, IL).

D-[1-^{11}C]Glucose

The production of D-[1-^{11}C]glucose followed the method of Link et al. (*29*) as modified from Shiue and Wolf (*30*), with additional modifications introduced by Dence et al. (*31*).

D-[6-^{11}C]Glucose

The synthesis of D-[6-^{11}C]glucose was developed in our laboratory and has been reported in detail (*32*).

In Vitro Experiments

Monolayers. T-36B-10 glioma cells were incubated in 25-ml glass Erlenmeyer flasks in 2.5 ml serum-free Waymouth's medium with either 10 μCi [1-^{14}C]glucose or [6-^{14}C]glucose at 37°C (glucose concentration of 27 m*M*). All generated [^{14}C]CO_2 was trapped in a polypropylene well containing 0.2 ml Soluene-350, which was suspended above the cell-containing medium in the flasks. Incubation was terminated after 60 min by acidification of the medium with 0.5 ml 1 *N* perchloric acid. This was followed by incubation at 37°C for 19–24 hr to release all the [^{14}C]CO_2. The well with Soluene containing trapped CO_2 was added to 10 ml Instagel and counted. The radioactivity level was used to calculate the yield of CO_2 generated in nmole/hr. Protein content in the monolayers was determined by routine methods (*33*), and CO_2 production was expressed in nmole CO_2/mg protein/hr. The ratio of C-1 [^{14}C]CO_2/C-6 [^{14}C]CO_2 was then calculated (*24*).

Tissue Slices. The intracerebral tumor implants for this study were produced from in vitro stocks of T-36B-10 glioma that were prepared in suspension and then injected by the stereotaxic method of Barker et al. (*34*) as reported previously (*26*). After rapid killing and brain removal from rats bearing glioma grafts of 50–100 mg, slices of glioma or normal brain 1 mm thick were prepared. The slices were incubated as described above for the monolayers with either 10 μCi [1-^{14}C]glucose or [6-^{14}C]glucose. The generated [^{14}C]CO_2 was similarly trapped and quantified to yield the nmole CO_2 produced/mg wet weight of tissue/hr and the ratio of C-1 [^{14}C]CO_2/C-6 [^{14}C]CO_2 production.

Glucose Metabolic Rate In Vitro

The glucose uptake by monolayers of T-36B-10 was quantified so that the PC usage could be calculated as a percentage of total glucose utilization. Monolayers were incubated as above with [6-^{14}C]glucose for 15 sec and then rapidly rinsed and denatured with 1 *N* perchloric acid (n = 12). This produced cell lysates in which the glucose metabolites were determined by anion exchange chromatography (*28*). Protein content was determined by the method of Lowry et al. (*33*). The glucose utilization rate (MRGlc) was calculated as the rate of conversion of glucose to metabolites per milligram protein per hour. Along with the C-1 [^{14}C]CO_2 and C-6 [^{14}C]CO_2 data collected from monolayers as above, the PC fraction of total glucose utilization was estimated with the following formulas (*35*):

$$\frac{\left(\frac{\text{C-1 } CO_2}{\text{MRGlc}}\right) - \left(\frac{\text{C-6 } CO_2}{\text{MRGlc}}\right)}{1 - \left(\frac{\text{C-6 } CO_2}{\text{MRGlc}}\right)} = S \qquad \text{Eq. 1}$$

$$\%\ \text{PC} = \frac{100S}{3 - 2S}. \qquad \text{Eq. 2}$$

These expressions assume that glucose is metabolized entirely through the PC and EMP, i.e., that none is metabolized through

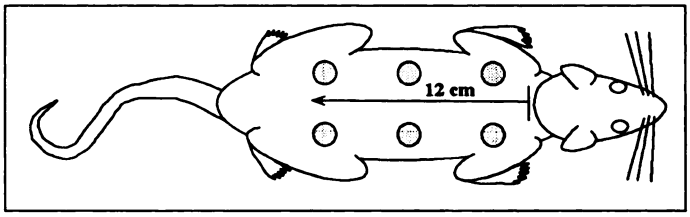

FIGURE 2. Pairs of bilateral subcutaneous grafts were placed on either dorsal side at 4, 8 and 12 cm caudal to the base of the skull. Each tumor was 2–3 cm from the midline.

nontriose-phosphate pathways. The ratio S/(3 − 2S) accounts for the different fates of the labeled glucose carbon atoms as they pass through the triose-phosphate reactions.

Statistical Analysis

The yields of CO_2 from C-1 label or C-6 label were compared by Student's t-test.

In Vivo Experiments

Tumor Implantation. Subcutaneous grafts of T-36B-10 glioma cells were produced by harvesting cells growing in culture, counting and injecting in 350-g F-344 male rats at six dorsal sites as illustrated (Fig. 2). Each transplant site received 5×10^5 cells in 0.1 ml carrier medium. The tumors were used for experiments 2–3 wk later when they reached 100–150 mg in size. The subcutaneous grafts of T-C6 glioma were similarly prepared except the cells were grafted in Wistar/Furth recipients.

There were two separate groups of T-36B-10-bearing rats prepared for the isotope injection experiments described below (Table 1): Group A unirradiated and Group B whole-body-irradiated with 10 Gy ^{137}Cs gamma rays, 1.6 Gy/min, 4 hr before the isotope injections to determine if irradiation would induce PC glucose metabolism. The rats bearing T-C6 glioma were studied without irradiation.

Animal Preparation for the Isotope Experiments

Under pentobarbital anesthesia (30 mg/kg, i.p.), polyethylene catheters (PE-10) were placed into the descending aorta through the femoral artery and into the inferior vena cava through the femoral vein (*28*). After this, the rats were allowed to awaken and adjust for 1 day before isotope studies. Food was withheld at least 12 hr before isotope injections.

Isotope Injection, Blood Sampling and Tissue Sampling

The rats were anesthetized with 30 mg/kg pentobarbital. They then received bolus injections containing either 20 μCi of D-[6-^{14}C]glucose and 600-1000 μCi of D-[1-^{11}C]glucose, or 20 μCi of D-[1-^{14}C]glucose and 300–500 μCi of D-[6-^{11}C]glucose through the femoral venous catheter in 150–600 μl of 0.9% saline (Table 1). Simultaneously, arterial blood sampling was started to generate an arterial plasma time-activity curve for each isotope. Samples (70 μl) were collected in microhematocrit tubes at 1, 2, 3, 4, 5, 7, 15, 25, 35, 45 and 55 min postinjection. The blood samples were centrifuged and 20 μl of the resulting plasma was counted for ^{11}C radioactivity in a gamma counter. After the decay of ^{11}C, the plasma samples were counted for ^{14}C as follows: 1 ml Soluene was added to each sample and allowed to digest overnight. The following were added before counting: one milliliter of 1 *N* HCl, 0.2 ml H_2O_2 and 10 ml of Instagel. Each sample was counted for 10 min or for a 2 σ level of 0.1% in a liquid scintillation counter (model 1900CA, Packard Instruments, Downers Grove, IL). We have examined the effect of neutralizing the Soluene-digested samples with acid and found that the activity in plasma and tissue samples changed linearly by no more than 0.4% at 30 min, which had no significant effect on the modeling results below.

In each rat, one tumor was ligated and sampled at each of the following times after isotope injection: 7, 15, 25, 35, 45 and 55 min. Each sample was placed in an appropriately labeled and preweighed counting vial. At 55 min, the animals were killed; samples of brain and masseter muscle were then also collected. Tissue ^{11}C radioactivity levels were counted as above. Thereafter 1.0 ml Soluene was added to dissolve each sample. The samples were then transferred to glass scintillation vials and were processed similar to the plasma samples.

The six tumors from each rat yielded tumor time-activity curves for ^{11}C and ^{14}C, which were normalized to the respective arterial plasma time-activity curves in order to determine differences in the amount of either label taken up and retained in the tumors. The area under the curve (AUC) was computed by trapezoidal integration. The percent difference between the C-6 AUC and the C-1 AUC was calculated as:

$$\% \text{ Difference in AUC} = \frac{(\text{C-6 AUC} - \text{C-1 AUC})}{\text{C-6 AUC}} \times 100. \quad \text{Eq. 3}$$

From this, the average percent difference was determined for each group. The one-tailed, paired Student's t-test was used to test the null hypothesis that the difference (C-6 AUC − C-1 AUC) was zero in each experimental group.

The ratio of C-1 retention relative to C-6 retention, the C-1/C-6 ratio, was calculated for all tumors as well as for the 55 min time point for brain and muscle samples. The difference between irradiated and unirradiated brain and muscle samples was assessed by Student's t-test.

To rule out the possibility that PC glucose metabolism in red blood cells (RBCs) contributed to our plasma or tissue radioactivity data, we examined the relative utilization of [1-^{11}C]glucose and [6-^{14}C]glucose in the RBC of nontumor-bearing rats. Seven animals received simultaneous intravenous injections of 1000 μCi [1-^{11}C]glucose and 10 μCi [6-^{14}C]glucose at time zero, after which arterial blood samples were collected after 10, 20, 30, 40, 50 and 60 min. Whole-blood and RBC radioactivity were measured as above. The ratio of C-1 to C-6 radioactivity in the RBC was calculated and plotted against the time of sample collection to determine if there was any decline from unity that could be due to PC metabolism.

TABLE 1
Grouping of All Animals Used in the In Vivo Experiments

Experimental group	Tumor	Number of graft sites/rat	Number of rats per group	Irradiation	Isotopes injected
A	T-36B-10	6	6	None	[1-^{11}C]-glc + [6-^{14}C]-glc
B	T-36B-10	6	6	10 Gy whole-body	Same as A
C	T-C6	6	6	None	Same as A (three rats) or [6-^{11}C]-glc + [1-^{14}C]-glc (three rats)

glc = glucose.

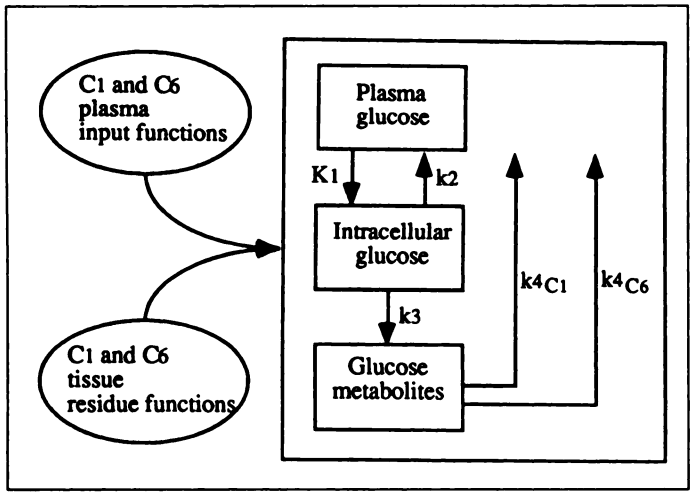

FIGURE 3. Three-compartment mathematical model of glucose metabolism.

Mathematical Modeling

A three-compartment model describing the kinetics of both C-1 glucose and C-6 glucose is shown diagrammatically in Figure 3. It is based on the work of Blomqvist et al. (*36*), who described a similar model for human brain PET studies with [1-^{11}C]glucose. The term, k4, accounts for loss of activity from the tissue as CO_2 through the PC or TCA cycle or as other intermediates such as lactate. The model was implemented with two plasma input functions and two output tissue functions, one pair for the C-1 and one pair for the C-6 glucose. The parameters, K1, k2, k3 and blood volume, were constrained to be identical for the two hexoses, whereas the k4 parameter was independently optimized for each residue function to yield $k4_{C1}$ and $k4_{C6}$. The model output was fit to the tissue data using nonlinear optimization to generate estimates of the six parameters. The difference ($k4_{C1} - k4_{C6}$) was determined for each animal and the percent difference of $k4_{C1}$ from $k4_{C6}$ was computed as:

$$\% \text{ Difference in k4} = \frac{(k4_{C1} - k4_{C6})}{k4_{C6}} \times 100. \qquad \text{Eq. 4}$$

A paired, one-tailed Student's t-test was used to test the null hypothesis that the difference between $k4_{C1}$ and $k4_{C6}$ was zero. This approach was chosen because the data are paired and because $k4_{C1}$ can only be higher than $k4_{C6}$, based on the potential loss of C-1 label from glucose but not the C-6 label in the PC pathway of glucose metabolism beyond the glucose-6-phosphate step. The Student's t-test assumes that the data follow a Gaussian distribution. The data were examined for deviation from this assumption using a Shapiro-Wilkes procedure, and in no case was the assumption rejected.

Once the parameter values were estimated for the series of rat tumors, these values were used to set up a repetitive Monte Carlo program to determine the feasibility of quantitatively imaging PC metabolism in a human patient using PET with successive injections of [1-^{11}C]glucose and [6-^{11}C]glucose and a region of interest (ROI) containing malignant glioma tissue. A smooth plasma input function for each glucose, C-1 or C-6, obtained from [1-^{11}C]glucose human PET studies, and rat glioma parameter values for K1, k2 and k3 were entered in the program. Specifically, these K1, k2 and k3 parameters were average values from the T-36B-10 and T-C6 data, excluding the irradiated T-36B-10 group. From results shown below, the value of $k4_{C6}$ was set at 0.025 min^{-1}, whereas $k4_{C1}$ was set at three levels for three separate runs, namely, 0.025, 0.0275 and 0.03, so that $k4_{C1}/k4_{C6}$ = 1.0, 1.1 and 1.2, respectively. The program then calculated two noise-free tissue outputs. Noise was then added to these outputs to simulate the stochastic noise that arises from PET imaging. The noise was set to simulate conditions in a PET study of a 70-kg human with an injection of 20 mCi each of [1-^{11}C]glucose and [6-^{11}C]glucose and a glioma ROI of 10 ml. This was based on observed counting rates from several human studies with [1-^{11}C]glucose. The simulated imaging time for each tracer was 60 min with the second injection occurring 60 min after the first. The Levenberg-Marquardt optimizer then adjusted the parameter values (K1, k2, k3, $k4_{C1}$, $k4_{C6}$, blood volume) to obtain a best fit to the noisy tissue data (*37*). Each of the three runs consisted of 2000 repetitions to obtain distributions of parameter estimates. The outputs were plotted as $k4_{C1}$ versus $k4_{C6}$.

Additionally, the Monte Carlo program was implemented as above with parameter values reported from human PET studies with [1-^{11}C]glucose (K1 = 0.083 ml/g/min, k2 = 0.33 min^{-1} and k3 = 0.35 min^{-1}) (*36*), while we set Vpv = 0.04 ml/g. The value of $k4_{C6}$ was set at 0.01 min^{-1}, whereas $k4_{C1}$ was set at three levels for the three separate runs, namely, 0.01, 0.011 and 0.012, so that $k4_{C1}/k4_{C6}$ = 1.0, 1.1 and 1.2, respectively.

ROC curves were constructed from the distribution of the ratio of estimated $k4_{C1}/k4_{C6}$ when the ratio was greater than 1.0, compared to the distribution when the ratio was equal to 1.0, the ratio expected if there were no PC metabolism. The ROC curves were constructed by determining the true-positive and false-positive ratios for several different discrimination levels (*38*).

TABLE 2
CO_2 Production Results for the Experiments In Vitro

	$^{14}CO_2$ from [1-^{14}C]glucose*	$^{14}CO_2$ from [6-^{14}C]glucose	C-1/C-6 ratio†
T-36B-10 glioma monolayers‡	40.4 ± 2.0§	4.6 ± 0.0	8.8
Intracerebral glioma slices¶	1.06 ± 0.14§	0.18 ± 0.04	6.1
Normal brain slices¶	0.34 ± 0.11	0.32 ± 0.11	1.1

*Means ± s.d.; n = 3 for each group.
†Ratio of means.
‡Nanomoles of [^{14}C]CO_2 produced per milligram protein per hour.
§$p < 0.005$, C-1 versus C-6 glucose.
¶Nanomoles of [^{14}C]CO_2 produced per milligram wet weight of tissue per hour.

RESULTS

In Vitro Experiments

These experiments quantified the [^{14}C]CO_2 generation from monolayers of T-36B-10, tumor slices of T-36B-10 or normal brain slices after incubation in medium containing either [1-^{14}C]glucose or [6-^{14}C]glucose (Table 2). The glioma monolayers and slices both showed significantly more CO_2 production from C-1 than from C-6-labeled glucose, indicating PC metabolism ($p < 0.005$). This result was in marked contrast to normal brain slices, which did not not indicate PC metabolism.

The glucose uptake (MRGlc) in T-36B-10 glioma monolayers was 707 ± 72 (s.d.) nmole/mg protein/hr (n = 12). Along with the C-1 [^{14}C]CO_2 and C-6 [^{14}C]CO_2 data above, the PC fraction of total glucose metabolism was calculated to be 1.8 ± 0.5% (s.d.).

In Vivo Experiments

Figures 4a and 4b show the results in the T-36B-10 experiments from six unirradiated rats (Fig. 4a) and six whole-body-irradiated rats (Fig. 4b). The tumor radioactivity concentration was normalized to the plasma time-activity curve for the respective isotopes and plotted against time after injection. In each graph, the C-6 tissue curve is higher than the C-1 curve. The difference between the C-6 AUC and the C-1 AUC is 4.9%

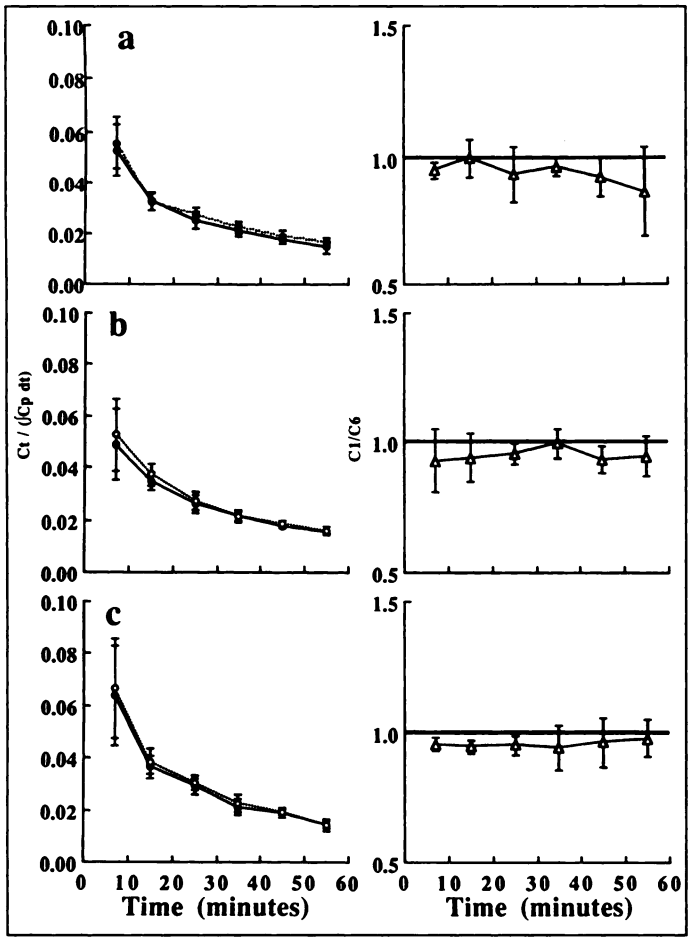

FIGURE 4. Left: Plots of normalized tumor radioactivity versus time of tumor sampling for glucose labeled in either the C-1 (——) or C-6 position (·····). The C-1 curves remain lower than the C-6 curves, indicating greater loss of C-1 relative to C-6 from the tumors. Right: Data are presented as the C1/C6 ratio (——) that remains less than one at all time points. (a) T-36B-10 glioma (n = 6), (b) Irradiated T-36B-10 glioma (n = 6) and (c) T-C6 glioma (n = 6). Error bars are 1 s.d.

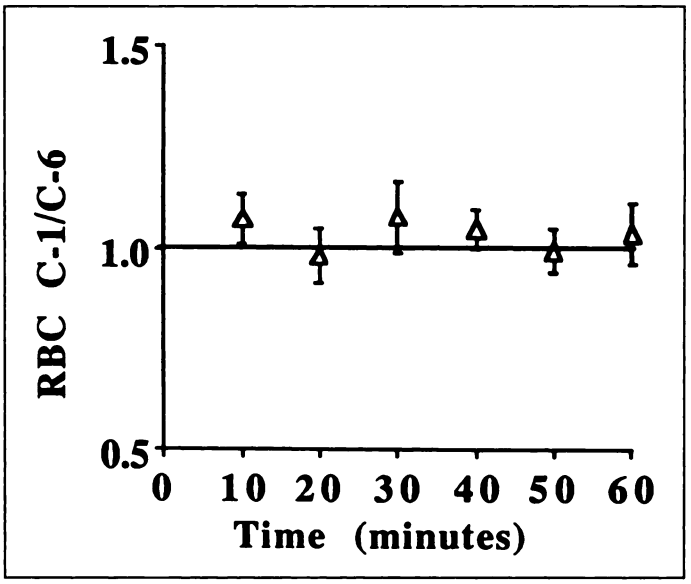

FIGURE 5. The ratio of C-1 relative to C-6 retention in RBCs of nontumor-bearing rats injected i.v. simultaneously with [1-^{11}C]glucose and [6-^{14}C]glucose (n = 7).

for unirradiated T-36B-10 glioma (Fig. 4a) ($p < 0.01$) and 5.6% for the irradiated group (Fig. 4b) ($p < 0.05$).

Figure 4c shows the results for six rats implanted with T-C6 glioma and left unirradiated. The difference between the C-6 AUC and the C-1 AUC is 4.7% ($p < 0.01$).

In the experiment designed to examine the potential effect of RBC PC utilization on our plasma and tumor tissue radioactivity data, there was essentially no deviation of the RBC C-1/C-6 ratio from unity over the hour studied (Fig. 5). This effectively ruled out PC metabolism in RBC as an explanation for the results graphed in Figure 4.

The data shown in Figure 4 were analyzed with parameter optimization and a model of glucose metabolism that simultaneously optimized C-1 and C-6 glucose kinetics by fitting the output to the C-1 and C-6 tumor time-activity curves. The parameters, K1, k2, k3 and k4, are shown in Tables 3 and 4. The rate constant for exchange of glucose metabolites from tumor to plasma, k4, i.e., loss of isotopic carbon from the tumors, was higher for C-1 than C-6 in all groups of rats—19% for T-36B-10 unirradiated, $p = 0.06$; 32% for T-36B-10 irradiated, $p = 0.03$; and 32% for T-C6, $p = 0.02$.

After K1, k2, k3 and k4 were estimated from parameter optimization and modeling, they were used for the Monte Carlo simulations. From the T-36B-10 and T-C6 data, excluding the irradiated T-36B-10, average values of K1, k2 and k3 were used, namely, 0.038, 0.118 and 0.342, respectively. $k4_{C1}$ was set at 0.025, 0.0275 or 0.03 for three separate runs, whereas $k4_{C6}$ was set at 0.025 for all runs such that the ratio, $k4_{C1}/k4_{C6}$, was varied from 1.0–1.2. The simulations are shown in Figures 6a, b, c as plots of the estimated $k4_{C1}$ and $k4_{C6}$ for the three runs. The simulations assumed a 20-mCi injection of [1-^{11}C]glucose followed by 20 mCi [6-^{11}C]glucose in a human subject. The ROC curve that illustrates the ability to discriminate the ratio of 1.1 is shown in Figure 7. Assuming the $k4_{C1}/k4_{C6}$ ratio is 1.1 and setting a threshold level at 1.05, it should be possible to detect the presence of PC activity in a 10-ml tumor volume with a sensitivity of 0.93 and a specificity of 0.91.

The Monte Carlo simulations were repeated with human parameter values reported by Blomqvist et al. (*36*) (K1 = 0.083 ml/g/min, k2 = 0.33 min^{-1} and k3 = 0.35 min^{-1}). The value of $k4_{C6}$ was set at 0.01 min^{-1}, whereas $k4_{C1}$ was set at three levels for the three separate runs, namely, 0.01, 0.011 and 0.012, so that again $k4_{C1}/k4_{C6}$ = 1.0, 1.1 and 1.2, respectively. Under these conditions, assuming the $k4_{C1}/k4_{C6}$ ratio is 1.2 and setting a threshold level at 1.10, it should be possible to detect the presence of PC activity in tumor with a sensitivity of 0.93 and a specificity of 0.92 (Fig. 8). For a $k4_{C1}/k4_{C6}$ ratio of 1.1 and a threshold level at 1.06, the sensitivity is 0.75 and the specificity is 0.80.

The C-1/C-6 ratio was calculated for the 55-min time point for the brain and muscle samples from 13 unirradiated and 9 irradiated rats. This ratio equaled 0.97 ± 0.10 (s.d.) and 0.99 ± 0.15 for unirradiated and irradiated brains, respectively, not significantly different from each other ($p = 0.77$). For the muscle the ratio was 1.03 ± 0.11 and 1.05 ± 0.18 for unirradiated and irradiated samples, respectively, which also was not a significant difference ($p = 0.76$).

TABLE 3
Mean (s.d.) K1, k2 and k3 Values Derived by Parameter Optimization

Tumor	K1	k2	k3
T-36B-10	0.036 (0.005)	0.152 (0.058)	0.418 (0.130)
T-36B-10, irradiated	0.036 (0.004)	0.085 (0.082)	0.300 (0.206)
T-C6	0.040 (0.008)	0.084 (0.061)	0.266 (0.226)

TABLE 4
$k4_{C1}$ and $k4_{C6}$ Mean Values

Tumor	$k4_{C1}$	$k4_{C6}$	$k4_{C1} - k4_{C6}$ (± s.e.m.)*	p value†
T-36B-10	0.019	0.016	0.003 (±0.002)	0.06
T-36B-10, irradiated	0.028	0.022	0.007 (±0.003)	0.03
T-C6	0.041	0.031	0.010 (±0.003)	0.02

*Average of individual differences, not difference of means.
†Determined by Student's paired, one-tailed t-test.

DISCUSSION

The results of our experiments in vitro show a 6- to 8-fold increase in PC utilization in T-36B-10 compared to normal brain. This utilization in vitro represents 1.8% of the total glucose metabolism in the glioma. The findings of other in vitro studies are similar. Coleman and Allen (*9*) performed $[^{14}C]CO_2$ generation studies on slices of five brain and three spinal cord ethylnitrosourea-induced rat gliomas and showed that the ratio of C-1/C-6 CO_2 production was 3.2 in the brain tumors and 6.3 in the spinal cord tumors. With their measurement of glucose utilization by the gliomas, viz., 15 μmole/g/hr, it is possible to calculate the fraction of PC utilization relative to total glucose metabolism in their gliomas by the approach of Katz and Wood (*35*). This results in 2%–3%, which agrees very well with the 1.8% we found in T-36B-10 in vitro. From their data on normal adult brain in vitro similarly calculated, the PC fraction was 0.5%.

Kingsley-Hickman et al. (*20*) and Ross et al. (*21*) estimated the fraction of PC glucose metabolism in T-9L gliosarcoma and T-C6 glioma in vitro by means of ^1H nuclear magnetic resonance spectroscopy or gas chromatography-mass spectrometry. With these techniques, the cells are exposed to either [1-^{13}C]glucose or [6-^{13}C]glucose while the differential production of [3-^{13}C]lactate or [3-^{12}C]lactate is measured. They found the percentage PC activity in T-9L to be 5.1 ± 1.2% (s.d.) and 7.5 ± 1.5% in T-C6.

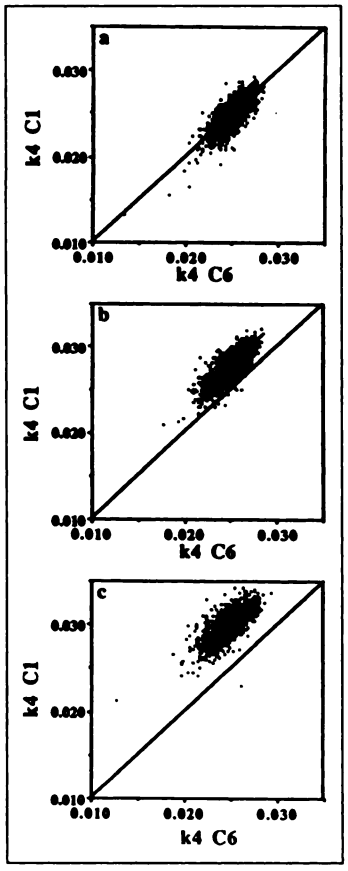

FIGURE 6. Plots of the distribution of $k4_{C1}$ versus $k4_{C6}$ derived from the Monte Carlo simulations in reference to the line of identity. (a) nominal $k4_{C1}$ = 0.025, $k4_{C6}$ = 0.025; (b) nominal $k4_{C1}$ = 0.0275, $k4_{C6}$ = 0.025; and (c) nominal $k4_{C1}$ = 0.03, $k4_{C6}$ = 0.025.

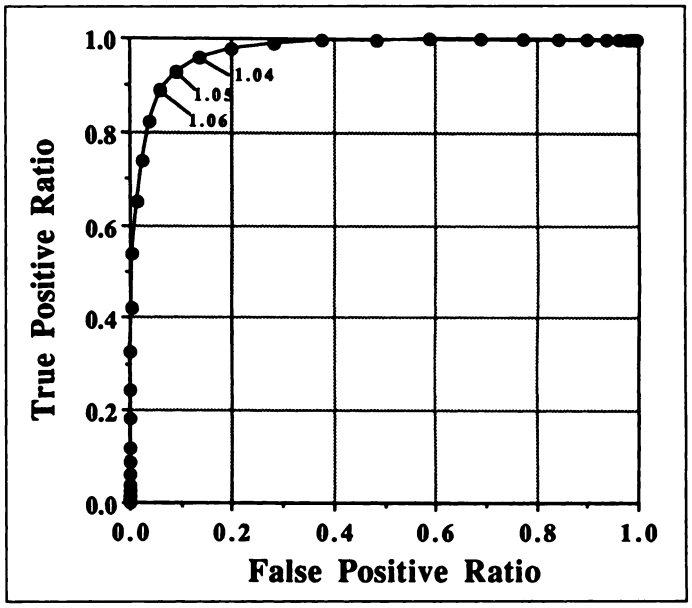

FIGURE 7. ROC curve for $k4_{C1}/k4_{C6}$ = 1.1 based on rat glioma rate constant values. This curve shows the trade-off between sensitivity (true-positive) and specificity (1 − false-positive) for detecting the presence of PC activity when 10% of total glucose metabolism is through the PC.

The results from our experiments in vivo with the T-36B-10 glioma demonstrate that the C-1-labeled carbon produced by PC metabolism is lost from the tumor tissue more rapidly than the C-6-labeled carbon. The curves in Figure 4a show a small but detectable difference between the behavior of C-1- and C-6-labeled glucose in unirradiated tumors. The curves for T-C6 glioma (Fig. 4c) demonstrate a difference between C-1- and C-6-labeled glucose similar to that found in the T-36B-10 glioma. For T-36B-10, the C-1 AUC was 4.9% lower than C-6, and for T-C6 glioma, the C-1 AUC was 4.7% lower ($p < 0.01$). We detected no increase in the PC in T-36B-10 in response to 10 Gy

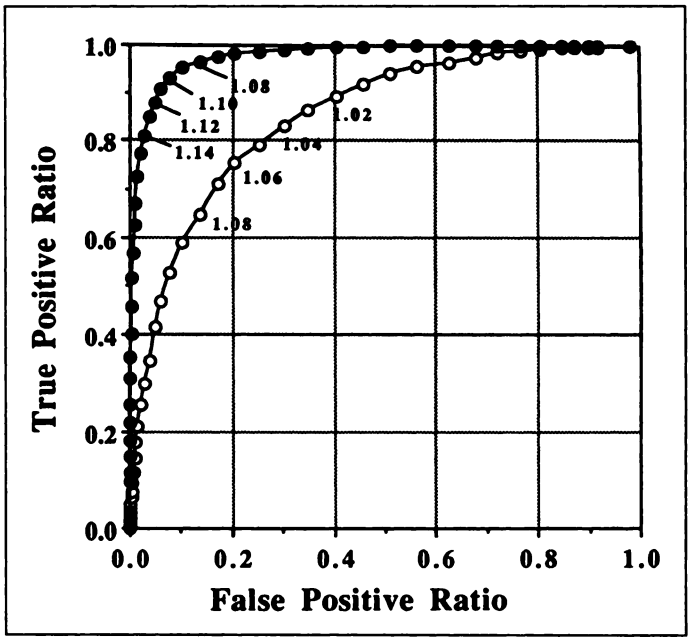

FIGURE 8. ROC curves for $k4_{C1}/k4_{C6}$ = 1.2 (●) or 1.1 (⊖) based on human rate constant values.

radiation exposure in vivo, although the C-1 AUC was 5.6% lower than the C-6 (Fig. 4b) ($p < 0.05$).

The object of our study was to explore in animal models the feasibility of using ^{11}C glucose labeled in the C-1 or C-6 position to quantify PC metabolism in human gliomas. The rat plasma and tumor time-activity data for C-1 and C-6 glucose provided the input for the kinetic model shown in Figure 3. This approach allowed us to estimate values of rate constants for loss of metabolites from the tumors for each of the labeled hexoses, $k4_{C1}$ or $k4_{C6}$ (Table 4). The Monte Carlo simulations using these rate constants showed the distribution of results that would be produced by a similar human study with a noise level in the range expected from a PET study with ^{11}C glucose, if a ROI contained 10 ml of tumor tissue. Based on these simulations, assuming conservatively the $k4_{C1}/k4_{C6}$ ratio equals 1.1, the ROC curve analysis indicates that it would be possible to detect the presence of PC activity in a 10-ml tumor ROI with a sensitivity of 0.93 and a specificity of 0.91 (Fig. 7). When the human rate constant values were used for the simulations assuming the $k4_{C1}/k4_{C6}$ ratio equals 1.2, the ROC curve analysis indicates that it would be possible to detect the presence of PC activity in a 10-ml tumor ROI with a sensitivity of 0.93 and a specificity of 0.92 (Fig. 8).

Numerous assumptions have been made to determine this sensitivity and specificity. The minor assumptions include the linear characteristics of the tomograph, accurate calibration, adequate description of noise levels and noise propagation and existence of significant PC activity in human tumors. The major assumption is that the glucose model used is sufficiently complete to predict the behavior of increased PC activity.

The model could be extended to include additional intermediates such as lactate and components of the TCA cycle. The problem with such extensions is that the number of unknown parameters rises, and it becomes impossible to achieve a unique solution. The model shown in Figure 3 is a good representation of the processes we are studying. The loss term (k4) includes CO_2 loss through the PC or TCA cycle or as other intermediates such as lactate. A late loss term (k5), along with delay, was originally included in the model to account for CO_2 loss after 2.5 turns of the TCA cycle or loss of labeled carbon metabolized through other intermediates. During optimization of data from human studies with [^{11}C] glucose, k5 always approached zero and so was not included in the final model.

At this time, the strongest support for this model is its success in a series of human studies of [1-^{11}C]glucose and FDG metabolism in normal brain regions in patients with gliomas (*39,40*). When the glucose metabolic rate is calculated from the model in Figure 3 with only one k4 and is compared to the FDG metabolic rate calculated with Phelp's (*41*) version of Sokoloff's model, the normal brain MRGlc is in the 25–28 μmole/100 g/min range, in excellent agreement with measurements by the Fick method (*36*). This suggests the model is sufficiently detailed for accurate calculations of metabolic rates and may well be adequate for the Monte Carlo predictions of the impact of PC activity on parameter estimates.

Further investigations are necessary to clarify the feasibility of imaging the PC with PET in human gliomas. The first is to examine several human gliomas in vitro as monolayers or slices to determine if they utilize the PC to a greater or lesser extent than we have found in the rat. The second step is to scan with PET several patients with malignant gliomas in two immediately successive [1-^{11}C]glucose studies to determine if the interstudy variation is smaller than the expected difference between successive studies with first [1-^{11}C]glucose then [6-^{11}C]glucose. If the human gliomas in vitro show increased PC utilization and successive [1-^{11}C]glucose PET studies show small interstudy variation, then it would be of great interest to synthesize sufficient [6-^{11}C]glucose and proceed to PET imaging of human gliomas comparing the kinetic parameters of [1-^{11}C]glucose and [6-^{11}C]glucose.

ACKNOWLEDGMENTS

We thank Dr. Anthony Shields for his critical review and suggestions. This work was supported by National Institutes of Health grant CA42045.

REFERENCES

1. Coleman RE, Hoffman JM, Hanson MW, Sostman HD, Schold SCJ. Clinical application of PET for the evaluation of brain tumors. *J Nucl Med* 1991;32:616–622.
2. Di Chiro G. Positron emission tomography using [^{18}F]fluorodeoxyglucose in brain tumors: a powerful diagnostic and prognostic tool. *Invest Radiol* 1987;22:360–371.
3. Glantz MJ, Hoffman JM, Coleman RE, et al. Identification of early recurrence of primary central nervous system tumors by [^{18}F]fluorodeoxyglucose positron emission tomography. *Ann Neurol* 1991;29:347–355.
4. Herholz K, Pietrzyk U, Voges J, et al. Correlation of glucose consumption and tumor cell density in astrocytomas. A stereotactic PET study. *J Neurosurg* 1993;79:853–858.
5. Tyler JL, Diksic M, Villemure JG, et al. Metabolic and hemodynamic evaluation of gliomas using positron emission tomography. *J Nucl Med* 1987;28:1123–1133.
6. Sokoloff L, Reivich M, Kennedy C, et al. The [^{14}C]deoxyglucose method for the measurement of local cerebral glucose utilization: theory, procedure and normal values in the conscious and anesthetized albino rat. *J Neurochem* 1977;28:897–916.
7. Weber G. Enzymology of cancer cells (first of two parts). *N Engl J Med* 1977;296: 486–492.
8. Weber G. Enzymology of cancer cells (second of two parts). *N Engl J Med* 1977;296:541–551.
9. Coleman MT, Allen N. The hexose monophosphate pathway in ethylnitrosourea induced tumors of the nervous system. *J Neurochem* 1978;30:83–90.
10. Hothersall JS, Baquer NZ, McLean P. Pathways of carbohydrate metabolism in peripheral nervous tissue. I. The contribution of alternative routes of glucose utilization in peripheral nerve and brain. *Enzyme* 1982;27:259–267.
11. Domanska-Janik K. Hexose monophosphate pathway activity in normal and hypoxic rat brain. *Resuscitation* 1988;16:79–90.
12. Zubairu S, Hothersall JS, El-Hassan A, McLean P, Greenbaum AL. Alternative pathways of glucose utilization in brain: changes in the pattern of glucose utilization and of the response of the pentose phosphate pathway to 5-hydroxytryptamine during aging. *J Neurochem* 1983;41:76–83.
13. Gaitonde MK, Evison E, Evans GM. The rate of utilization of glucose via hexose-monophosphate shunt in brain. *J Neurochem* 1983;41:1253–1260.
14. Loreck DJ, Galarraga J, Van der Feen J, Phang JM, Smith BH, Cummins CJ. Regulation of the pentose phosphate pathway in human astrocytes and gliomas. *Metab Brain Dis* 1987;2:31–46.
15. Allen N. Respiration and oxidative metabolism of brain tumors. In: Kirsch WM, Paoletti EG, Paoletti P, eds. *The experimental biology of brain tumors*. Springfield, IL: Charles C Thomas; 1972:243–274.
16. Lowry OH, Berger SJ, Carter JG, et al. Diversity of metabolic patterns in human brain tumors: enzymes of energy metabolism and related metabolites and cofactors. *J Neurochem* 1983;41:994–1010.
17. Marzatico F, Curti D, Dagani F, et al. Enzymes related to energy metabolism in human gliomas. *J Neurosurg Sci* 1986;30:129–132.
18. Timperley WR. Glycolysis in neuroectodermal tumors. In: Thomas DGT, Graham DI, eds. *Brain tumors, scientific basis, clinical investigation and current therapy*. London: Butterworths; 1980:145–167.
19. Coleman MT, Allen N. Activities of enzymes of the hexose monophosphate pathway in nervous system tumors induced by ethylnitrosourea. *Acta Neuropathol (Berlin)* 1978;41:223–227.
20. Kingsley-Hickman PB, Ross BD, Krick T. Hexose monophosphate shunt measurement in cultured cells with [1-^{13}C]glucose: correction for endogenous carbon sources using [6-^{13}C] glucose. *Anal Biochem* 1990;185:235–237.
21. Ross BD, Higgins RJ, Boggan JE, Willis JA, Knittel B, Unger SW. Carbohydrate metabolism of the rat C6 glioma. An in vivo ^{13}C and in vitro 1H magnetic resonance spectroscopy study. *NMR Biomed* 1988;1:20–26.
22. Hotta SS, Seventko JMJ. The hexosemonophosphate shunt and glutathione reduction in guinea pig brain tissue: changes caused by chlorpromazine, amytal and malonate. *Arch Biochem Biophys* 1968;123:104–108.
23. Hawkins RA, Mans AM, Davis DW, Vina JR, Hibbard LS. Cerebral glucose use measured with [^{14}C]glucose labeled in the 1, 2 or 6 position. *Am J Physiol* 1985:248;C170–C176.
24. Baquer NZ, Hothersall JS, McLean P. Function and regulation of the pentose phosphate pathway in brain. *Curr Top Cell Regul* 1988;29:265–289.
25. Benda P, Lightbody J, Sato G, Levine L, Sweet W. Differentiated rat glial cell strain in tissue culture. *Science* 1968;161:370–371.

26. Spence AM, Coates PW. Scanning electron microscopy of cloned astrocytic lines derived from ethylnitrosourea-induced rat gliomas. *Virchows Arch B Cell Pathol* 1978;28:77–85.
27. MacGregor RR, Fowler JS, Wolf AP, Shiue CY, Lade RE, Wan CN. A synthesis of 2-deoxy-D-[1-^{11}C]glucose for regional metabolic studies: concise communication. *J Nucl Med* 1981;22:800–803.
28. Spence AM, Graham MM, Muzi M, et al. Deoxyglucose lumped constant estimated in a transplanted rat astrocytic glioma by the hexose utilization index. *J Cereb Blood Flow Metab* 1990;10:190–198.
29. Link JM, Courter JH, Krohn KA. Remote automated synthesis of 1-[C-11]-D-glucose for patient imaging with PET. *J Nucl Med* 1989;30:928.
30. Shiue C-Y, Wolf AP. The synthesis of 1-[^{11}C]-D-glucose and related compounds for the measurement of brain glucose metabolism. *J Label Compds Radiopharm* 1985;22: 171–182.
31. Dence CS, Powers WJ, Welch MJ. Improved synthesis of 1-[^{11}C]D-glucose. *Appl Radiat Isot* 1993;44:971–980.
32. Grierson JR, Biskupiak JE, Link JM, Krohn KA. Radiosynthesis of 6-[C-11]-D-glucose. *Appl Radiat Isot* 1993;44:1449–1458.
33. Lowry OH, Rosebrough NJ, Farr AL, Randall RJ. Protein measurement with the Folin phenol reagent. *J Biol Chem* 1951;193:265–275.
34. Barker M, Hoshino T, Gurcay O, et al. Development of an animal brain tumor model and its response to therapy with 1,3-bis(2-chloroethyl)-1-nitrosourea. *Cancer Res* 1973;33:976–986.
35. Katz J, Wood HG. The use of $C^{14}O_2$ yields from glucose-1- and -6-^{14}C for the evaluation of the pathways of glucose metabolism. *J Biol Chem* 1963;238:517–523.
36. Blomqvist G, Stone-Elander S, Halldin C, et al. Positron emission tomographic measurements of cerebral glucose utilization using [1-^{11}C]D-glucose. *J Cereb Blood Flow Metab* 1990;10:467–483.
37. Press WH, Flannery BP, Teukolsky SA, Vetterling WT. *Numerical recipes in Pascal.* New York: Cambridge University Press; 1989.
38. Thompson ML, Zucchini W. On the statistical analysis of ROC curves. *Stat Med* 1989;8:1277–1290.
39. Spence AM, Graham MM, Muzi M, et al. Assessment of glucose metabolism in malignant gliomas: Use of deoxyglucose or glucose. Second European Workshop on FDG in Oncology. Heidelberg, Germany: 1991;9–11.
40. Spence AM, Muzi M, Graham MM, Freeman SD, Berger MS, Ojemann GA. Analysis of the deoxyglucose lumped constant in human malignant gliomas. *Ann Neurol* 1991;30:271–272.
41. Phelps ME, Huang SC, Hoffman EJ, Selin C, Sokoloff L, Kuhl DE. Tomographic measurement of local cerebral glucose metabolic rate in humans with (F-18)2-fluoro-2-deoxy-D-glucose: validation of method. *Ann Neurol* 1979;6:371–388.

Normal Fusion for Three-Dimensional Integrated Visualization of SPECT and Magnetic Resonance Brain Images

Rik Stokking, Karel J. Zuiderveld, Hilleke E. Hulshoff Pol, Peter P. van Rijk and Max A. Viergever
Image Sciences Institute and Department of Psychiatry, Utrecht University/University Hospital, Utrecht, The Netherlands

Multimodality visualization aims at efficiently presenting integrated information obtained from different modalities, usually combining a functional modality (SPECT, PET, functional magnetic resonance imaging) with an anatomical modality [CT, magnetic resonance imaging (MRI)]. This paper presents a technique for three-dimensional integrated visualization of SPECT and magnetic resonance brain images, where MRI is used as a framework of reference for the display of the SPECT data. **Methods:** A novel technique for three-dimensional integrated visualization of functional and anatomical information, called normal fusion, is presented. With this technique, local functional information is projected onto an anatomic structure. **Results:** The normal fusion technique is applied to three cases of SPECT/MRI integration. The results are presented, discussed and evaluated for clinical relevance. **Conclusion:** The results for three-dimensional integrated display of SPECT and MR brain images indicate that the normal fusion technique provides a potentially comprehensive and diagnostically valuable presentation of cerebral blood perfusion in relation to the anatomy of the brain.

Key Words: multimodality display; volume visualization; magnetic resonance imaging; SPECT; brain imaging

J Nucl Med 1997; 38:624–629

The use of multiple imaging modalities for clinical examinations is gradually increasing (*1,2*). The goals of multimodality visualization are to comprehensibly conjoin the diagnostic information of different imaging modalities and to communicate the integrated information to the referring specialists. The combination of complementary data from multiple modalities may reveal additional diagnostic information, as compared with interpretation directly from the individual imaging modalities (*3–7*). We distinguish two types of multimodality integration: (a) the combination of anatomical data from different modalities and (b) the combination of functional and anatomical data.

An example of the integration of multimodal anatomical information is the fusion of computed tomography (CT) and magnetic resonance imaging (MRI) in skull base surgery, where the combination is used to determine the precise location of a lesion (MRI data) with respect to bone (CT data) to obtain a more accurate diagnosis and treatment (*8*). Other examples of CT/MRI fusion, e.g., for radiation therapy planning, can be found (*9–13*).

Multimodality display can also integrate functional information from, e.g., PET, SPECT, electroencephalography, magnetoencephalography, magnetic resonance spectroscopy or functional MRI with anatomical information from MRI or CT (*2,5,14–17*). The anatomical modality then provides a frame of reference for spatially correct interpretation of the functional information. Valentino et al. (*6*) states: "In brain imaging in particular, the accurate display of functional and anatomic image data is essential in identifying sites of normal and pathophysiologic function in the brain."

This article addresses a novel technique for three-dimensional integrated display of SPECT and magnetic resonance (MR) brain images. When using SPECT in isolation, investigation of functional processes and the correlation with anatomical structures is hampered by the low spatial resolution (*16,18,19*). Two options can be utilized to facilitate the SPECT study: (a) the use (and manipulation) of color-encoding to display the SPECT data to exploit the potential of the visual system more effectively (*18*) and (b) visual comparison of SPECT perfusion images in pertinent cerebral regions with the homologous regions of the con-

Received Nov. 10, 1996; revision accepted Jul. 8, 1996.
For correspondence or reprints contact: Rik Stokking, University Hospital Utrecht, E 01.334, Heidelberglaan 100, 3584 CX Utrecht, The Netherlands.